

Article

A TIPS-TPDO-tetraCN-Based *n*-type Organic Field-Effect Transistor with a Cross-linked PMMA Polymer Gate Dielectric

Sungyeop Jung, Mohammed Albariqi, Guillaume Gruntz, Thamer AL HATHAL, Alba Peinado, Enric Garcia-Caurel, Yohann Nicolas, Thierry Toupance, Yvan Bonnassieux, and Gilles Horowitz

ACS Appl. Mater. Interfaces, **Just Accepted Manuscript** • DOI: 10.1021/acsami.6b00480 • Publication Date (Web): 18 May 2016Downloaded from <http://pubs.acs.org> on May 19, 2016**Just Accepted**

“Just Accepted” manuscripts have been peer-reviewed and accepted for publication. They are posted online prior to technical editing, formatting for publication and author proofing. The American Chemical Society provides “Just Accepted” as a free service to the research community to expedite the dissemination of scientific material as soon as possible after acceptance. “Just Accepted” manuscripts appear in full in PDF format accompanied by an HTML abstract. “Just Accepted” manuscripts have been fully peer reviewed, but should not be considered the official version of record. They are accessible to all readers and citable by the Digital Object Identifier (DOI®). “Just Accepted” is an optional service offered to authors. Therefore, the “Just Accepted” Web site may not include all articles that will be published in the journal. After a manuscript is technically edited and formatted, it will be removed from the “Just Accepted” Web site and published as an ASAP article. Note that technical editing may introduce minor changes to the manuscript text and/or graphics which could affect content, and all legal disclaimers and ethical guidelines that apply to the journal pertain. ACS cannot be held responsible for errors or consequences arising from the use of information contained in these “Just Accepted” manuscripts.

A TIPS-TPDO-tetraCN-Based n -Type Organic Field-Effect Transistor with a Cross-linked PMMA Polymer Gate Dielectric

Sungyeop Jung,^{*,†} Mohammed Albariqi,^{†,‡} Guillaume Gruntz,[¶] Thamer Al-Hathal,^{†,‡} Alba Peinado,[†] Enric Garcia-Caurel,[†] Yohann Nicolas,[¶] Thierry Toupance,[¶] Yvan Bonnassieux,[†] and Gilles Horowitz[†]

[†]*Laboratoire de Physique des Interfaces et des Couches Minces (LPICM), UMR CNRS 7647, École polytechnique, Université Paris-Saclay, 91128 Palaiseau Cedex, France*

[‡]*Royal Saudi Naval Forces, King Abdul Aziz Road, Dubbat, 12622 Riyadh, Saudi Arabia*

[¶]*Institut des Sciences Moléculaires (ISM), UMR CNRS 5255, University of Bordeaux, 33405 Talence Cedex, France*

E-mail: sungyeop.jung@polytechnique.edu

Abstract

Recent improvement in the performance of the n -type organic semiconductors as well as thin gate dielectrics based on cross-linked polymers offers new opportunities to develop high-performance low-voltage n -type OFETs suitable for organic complementary circuits. Using TIPS-tetracyanotriphenodioxazine (TIPS-TPDO-tetraCN) and cross-linked poly(methyl methacrylate) (c-PMMA), respectively as n -type organic semiconductor and gate dielectric, linear regime field-effect mobility $(1.8 \pm 0.2) \times 10^{-2} \text{ cm}^2 \text{ V}^{-1} \text{ s}^{-1}$, small spatial standard deviation of threshold voltage ($\sim 0.1 \text{ V}$), and operating voltage less than 3 V are attainable with the same device structure and contact

1
2
3 materials used commonly for *p*-type OFETs. Through comparative static and dy-
4
5
6
7
8
9
10
11
12
13
14
15
16
17
18
19
20
21
22
23
24
25
26
27
28
29
30
31
32
33
34
35
36
37
38
39
40
41
42
43
44
45
46
47
48
49
50
51
52
53
54
55
56
57
58
59
60

materials used commonly for *p*-type OFETs. Through comparative static and dynamic characterizations of c-PMMA and PMMA gate dielectrics, it is shown that both smaller thickness and larger relative permittivity of c-PMMA contributes to reduced operating voltage. Furthermore, negligible hysteresis brings evidence to small trap states in the semiconductor near gate dielectric of the *n*-type OFETs with c-PMMA. The use of TIPS-TPDO-tetraCN and c-PMMA is fully compatible with polyethylene terephthalate substrate, giving promise to various flexible applications.

Keywords

n-type organic field-effect transistors (OFETs), triphenyldioxazines (TPDOs), cross-linked polymer gate dielectrics, poly(methyl methacrylate) (PMMA), flexible electronics

1 Introduction

Organic field-effect transistors (OFETs) were firstly demonstrated in 1986 using electrochemically polymerized polythiophene as a *p*-type (hole-transporting) organic semiconductor.¹ Later in the early 1990's, with the discovery of *n*-type (electron-transporting) behavior in organic semiconductors, such as lutetium diphthalocyanine,² C₆₀^{3,4} or those bearing electron withdrawing groups such as cyanide⁵ or imide,^{6,7} research on *n*-type OFETs has attracted much attention⁸⁻¹⁰ leading to the rationalization of their operating mechanism which asserts on the minimum difference between the electron affinity of organic semiconductor and work function of source and drain contact metal as well as low reactivity between both materials.¹¹

The *n*-type OFETs are especially useful for organic complementary circuits (OCCs). Indeed, compared to the unipolar circuits based only on *p*-type OFETs, the use of both *n*- and *p*-type OFETs enables larger noise margin and lower power consumption.^{12,13} However, the early *n*-type organic semiconductors were highly sensitive to ambient air, humidity and light. In this respect, over the past two decades, developing a *n*-type organic semiconductor

1
2
3 with good stability and electron-transporting behavior has been one of the first priorities for
4 the improvement of the *n*-type OFETs.^{14,15}
5
6

7 So far, a modest number of *n*-type organic semiconductors have been reported to exhibit
8 good stability with improved electron mobility reaching occasionally $0.1 \sim 1 \text{ cm}^2\text{V}^{-1}\text{s}^{-1}$
9 (measured from *n*-type OFET mostly with a self-assembled monolayer (SAM)), which is
10 close to the hole mobility of evaporated *p*-type OFETs based on pentacene.¹⁶ Among them,
11 the perylene and naphthalene carboxydiimide derivatives are two famous families of *n*-type
12 organic semiconductors.¹⁷⁻²¹
13
14
15
16
17
18

19 At the same time, electron-transporting triphenodioxazine (TPDO) derivatives, which
20 can be produced at the industrial scale, have gain significant attention.^{22,23} A recent work
21 showed that air stability, solubility and electron-transporting behavior of TPDO derivatives
22 can be improved through substitution of TPDO core by nitrile and triisopropylsilylethynyl
23 (TIPS) groups.²⁴
24
25
26
27
28
29

30 On the other hand, a reliable gate dielectric, the easy processing of which is still actively
31 investigated, constitutes a key element for achieving low-voltage operation of the *n*-type
32 OFETs. The operating voltage is concerned with the thickness d_i and relative permittivity
33 (dielectric constant) ϵ_r of the gate dielectric because the drain current is proportional to
34 gate dielectric capacitance density $C_i = \epsilon_r \epsilon_0 / d_i$.²⁵ The state-of-the-art technologies on the
35 gate dielectrics at process temperature below 150°C comprise the use of high permittivity
36 metal oxides,²⁶ nanometer-thick SAMs (2~3 nm when used alone²⁷ or around 6 nm with
37 AlO_x ^{20,28}), organic-inorganic hybrid multilayer in few nanometer thickness²⁹ and thin cross-
38 linked polymers.³⁰⁻³³
39
40
41
42
43
44
45
46
47

48 It should bear in mind that the gate dielectric layer is critical not only for low-voltage
49 operation but also for other transistor parameters such as mobility and threshold voltage.
50 For example, the effect of the choice of polymer gate dielectric material on the growth
51 mechanisms has been recognized.^{30,31} A recent demonstration on the optimum combination
52 of organic semiconductors and nanometer-thick SAM gate dielectrics³⁴ emphasizes again the
53
54
55
56
57
58
59
60

1
2
3 importance of the right choice of a gate dielectric material.
4

5 In this paper, we report on *n*-type OFETs based on the TIPS-tetracyanotriphenodioxazine
6 (TIPS-TPDO-tetraCN) with the highest saturation mobility $\mu_{\text{sat}} = 0.1 \text{ cm}^2\text{V}^{-1}\text{s}^{-1}$ on a
7 SAM ever reported for TPDO derivatives.²⁴ The benefits of using a cross-linked poly(methyl
8 methacrylate) (c-PMMA) compared with a neat poly(methyl methacrylate) (PMMA) as a
9 gate dielectric material are thoroughly shown by electrical characterization of Al/gate dielec-
10 tric/Al capacitors and *n*-type OFETs as well as surface characterization of gate dielectric and
11 semiconductor layers. The Fourier transform infra-red spectroscopic Mueller ellipsometry is
12 employed to confirm the successful cross-linking. In addition to the mobility and operating
13 voltage, the performance of such *n*-type OFETs are analyzed in terms of other specifications
14 required for circuit applications such as minimum hysteresis and small spatial distribution of
15 threshold voltage, etc. In part, this study examines the TIPS-TPDO-tetraCN-based *n*-type
16 OFETs with c-PMMA on a polyethylene terephthalate (PET) substrate for flexible circuit
17 applications.
18
19
20
21
22
23
24
25
26
27
28
29
30
31
32
33

34 2 Experimental

35 2.1 Device structure

36
37
38 Figure 1a shows the devices architecture of a *n*-type OFET with bottom-gate/top-contact
39 (BG/TC) configuration. For gate and contact electrodes, aluminium (Al) and gold (Au)
40 were used, respectively, as commonly chosen for *p*-type OFETs. The channel length and
41 width were $L = 30, 40, 50, 60$ and $80 \mu\text{m}$ and $W = 1 \text{ mm}$. Figures 1b-d show the chemical
42 structures of TIPS-tetracyanotriphenodioxazine (TIPS-TPDO-tetraCN), PMMA and 1,6-
43 bis(trichlorosilyl)hexane ($\text{C}_6\text{-Si}$) used respectively as a *n*-type organic semiconductor, base
44 polymer for gate dielectrics and cross-linking agent for thin gate dielectric (c-PMMA). TIPS-
45 TPDO-tetraCN was synthesized according to a previously reported procedure.²⁴ PMMA
46 (MW = 120,000) and $\text{C}_6\text{-Si}$ were purchased from Sigma-Aldrich[®] and used without any
47
48
49
50
51
52
53
54
55
56
57
58
59
60

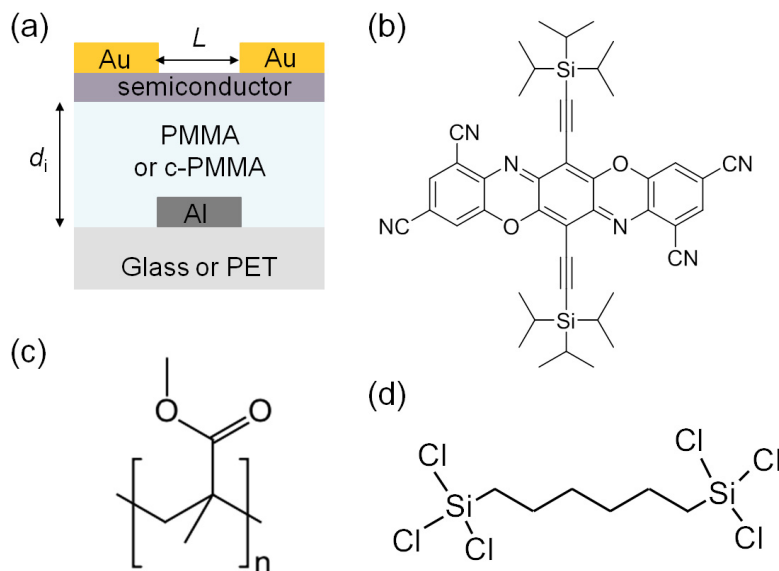


Figure 1: (a) Schematic diagram of the *n*-type organic field-effect transistors (OFETs) in bottom-gate/top-contact configuration. Chemical structures of (b) TIPS-tetracyanotriphenodioxazine (TIPS-TPDO-tetraCN), (c) poly(methyl methacrylate) (PMMA) and (d) 1,6-bis(trichlorosilyl)hexane (C_6 -Si) used respectively as a *n*-type organic semiconductor, base polymer for gate dielectrics and cross-linking agent for thin gate dielectric.

further purification. According to the combination of gate dielectrics, PMMA and c-PMMA, and substrates, glass and PET ($175\ \mu\text{m}$), four types of OFETs were systematically compared.

2.2 Device fabrication and characterization

Fabrication and characterization of OFETs The glass or PET substrates were cleaned successively with acetone, isopropanol and, finally, by a UV-ozone post-treatment. Then, the PET substrate was attached on a supporting glass substrate. Subsequent fabrication processes and characterizations of OFETs were carried out in a glove box under nitrogen atmosphere. The Al (gate electrode, 100 nm), TIPS-TPDO-tetraCN (organic semiconductor, 60 nm) and Au (contact electrodes, 30 nm) were thermally evaporated through a specific shadow mask. All evaporation processes were done under 1.9×10^{-7} mbar and fixed substrate temperature of 25°C . The evaporation rate of TIPS-TPDO-tetraCN was maintained at 0.01 nm/sec in average. Between the evaporation processes of Al and TIPS-TPDO-tetraCN, the

1
2
3
4 polymer gate dielectrics were spin-coated.

5 For PMMA gate dielectric, the PMMA solution (200 mg of PMMA dissolved in 3 ml of
6 toluene for 24 hours) was spin-coated at 3000RPM/5s/60s (Rotation Per Minutes/acceleration
7 time to reach the target RPM/spin-coating time). For cross-linked PMMA gate dielectric
8 (c-PMMA), 10 μ l of C₆-Si was introduced to the PMMA solution (25 mg of PMMA dissolved
9 for 40 min at 80°C in 1 ml of n-Butyl acetate and cooled down to 50°C) 2 min before spin-
10 coating at 5000RPM/5s/60s. After annealing at 100°C for 60 min, PMMA and c-PMMA
11 gate dielectrics have thickness of 510±10 and 100±16 nm (measured using a Dektak 150
12 surface profiler, Veeco).
13
14
15
16
17
18
19
20
21

22 Note that, in the work of Noh *et al.* on a cross-linked PMMA,³² the solution consisting
23 of the base polymer and cross-linking agent was prepared under nitrogen environment and
24 then spin-coated and post-annealed in air for a spontaneous cross-linking due to ambient
25 moisture. In this study, the whole spin-coating process was conducted in a glove box, which
26 is similar to the study of Yang *et al.*³⁵
27
28
29
30
31

32 All transfer and output characteristics of the *n*-type OFETs were measured with Keithley
33 4200 in the dark under nitrogen atmosphere directly after device fabrication without exposure
34 to air except for the air stability test. In particular, bending tests were performed with a
35 custom-built apparatus which consists of a hemicylindrical objects with different radii. The
36 transfer characteristics were measured while the devices were being bent. For the air stability
37 test, transistors were stored and measured in the dark under ambient atmosphere without
38 encapsulation.
39
40
41
42
43
44
45
46
47

48 **Fabrication of characterization of MIM capacitors** Vertical gate dielectric capaci-
49 tors (Al/gate dielectric/Al) in metal/insulator/metal (MIM) configuration were fabricated
50 through the same fabrication processes used for the OFETs. The static and dynamic char-
51 acterizations of the MIM capacitors were performed using a Keithley 4200 and a HP 4192A
52 LF impedance analyser in the dark under ambient air.
53
54
55
56
57
58
59
60

1
2
3 **Surface characterization** The surface properties of polymer gate dielectric and organic
4 semiconductor layers were analyzed by tapping mode atomic force microscope (AFM) using
5 Veeco Dimension 5000.
6
7
8

9
10
11 **Fourier transform infra-red (FTIR) spectroscopic Mueller ellipsometry** The pres-
12 ence of polysilsequioxane in c-PMMA polymer composite was studied by FTIR spectroscopic
13 Mueller ellipsometry. A customized equipment that combines FTIR spectroscope (Nicolet
14 6700) and a Mueller ellipsometer, sample preparation, raw data and extraction method of
15 optical constants are presented in the Supporting Information.
16
17
18
19
20
21

22 **3 Results and discussion**

23 **3.1 Electrical characteristics of gate dielectrics**

24
25
26
27 **Static characterizations** In order to evaluate the insulating properties of PMMA and
28 c-PMMA gate dielectrics, the current-voltage characteristics of gate dielectric capacitors
29 with PMMA or c-PMMA were measured (see Figure 2a). The inset of Figure 2 represents
30 the device structure of the vertical gate dielectric capacitors (Al/gate dielectric/Al) in MIM
31 configuration. The thickness of PMMA and c-PMMA insulator layers d_i is 510 ± 10 and
32 100 ± 16 nm. For a fair comparison of electrical rigidity, the applied voltage is normalized
33 by the thickness of each capacitor. It is observed that, for a practical range of electric
34 field (< 0.8 MV/cm) required for the sufficient charge carrier accumulation to create the
35 conducting channel, the leakage current density of c-PMMA capacitor is comparable to that
36 of PMMA capacitor despite of 5 times smaller thickness. The smooth surface characteristics
37 with no significant pinholes observed in AFM images of PMMA and c-PMMA layers (Figures
38 2c-d) explain their good electrical rigidity. The root mean square (RMS) values of PMMA
39 and c-PMMA layers are 0.4 and 1.3 nm. The depth of few pinholes observed in c-PMMA
40 layer (less than 5 nm) is negligible compared to the thickness of the c-PMMA (100 nm).
41
42
43
44
45
46
47
48
49
50
51
52
53
54
55
56
57
58
59
60

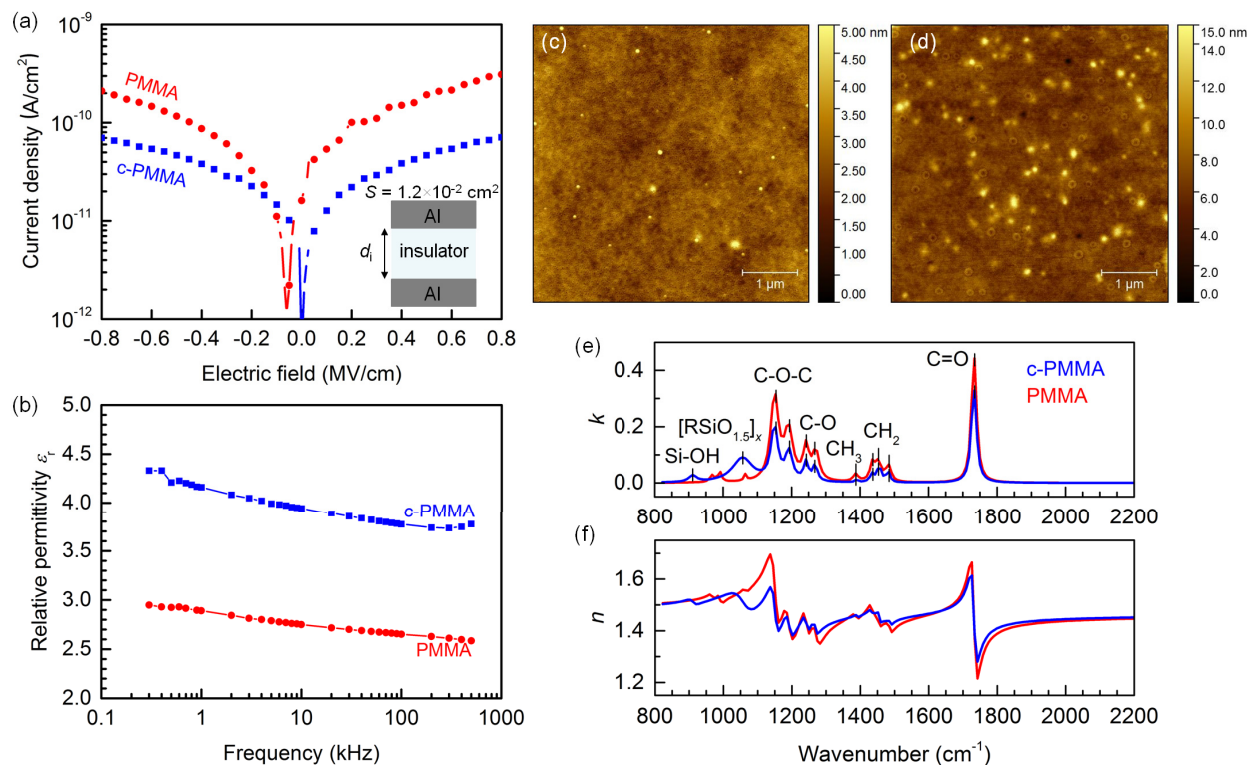


Figure 2: (a) Current density-electric field characteristics of vertical MIM capacitors (The inset represents the device structure. S and d_i denote the surface area of capacitor and the thickness of insulator layer.); (b) Relative permittivity ϵ_r measured by impedance spectroscopy; tapping mode AFM images of (c) PMMA and (d) c-PMMA gate dielectric layers on Al; (e) absorption coefficient k and (f) refractive index n of the gate dielectrics obtained by the FTIR spectroscopic Mueller ellipsometry.

FTIR spectroscopic Mueller ellipsometry The cross-linking chemical reaction of c-PMMA can be rationalized according to sol-gel polymerization of bridged trichlorosilane.³⁶ First, hydrolysis of C_6 -Si yields bis-(hydroxysilyl)hexane species with the concomitant release of hydrochloride acid. Then further nucleophilic substitution of chlorine atoms in C_6 -Si by silanol functions or condensation of silanol groups through oxolation reactions leads to 3-dimensional bridged polysilsesquioxane network. The latter then captures 1D-PMMA chains and densifies the final c-PMMA polymer composite which endows it with a higher electrical rigidity at smaller thickness than PMMA. The formation of the polysilsesquioxane in c-PMMA polymer composite was established by FTIR spectroscopic Mueller ellipsometry (Figures 2e-f). The typical features of PMMA (1734 ($\nu_{C=O}^{ester}$), 1484 - 1435 (δ_{CH_2}), 1395 (δ_{CH_3}), 1242 (ν_{C-O}^{ester}))

1
2
3 and 1145 (ν_{C-O-C}) cm^{-1}) were observed in the spectrum of c-PMMA as well as in that of
4
5
6
7
8
9
10
11
12
13
14
15
16
17
18
19
20
21
22
23
24
25
26
27
28
29
30
31
32
33
34
35
36
37
38
39
40
41
42
43
44
45
46
47
48
49
50
51
52
53
54
55
56
57
58
59
60
and 1145 (ν_{C-O-C}) cm^{-1}) were observed in the spectrum of c-PMMA as well as in that of
PMMA. Moreover, the presence of polysilsesquioxane species in c-PMMA was assessed by
the presence of additional broad vibrational bands at 1056 ($\nu_{[RSiO_{1.5}]_x}$) and 903 (δ_{Si-OH}) cm^{-1}
which clearly show the formation of the organic-inorganic hybrid layer.^{37,38} A more detailed
view of the cross-linking chemical reaction is given in the Supporting Information.

Dynamic characterizations Figure 2b shows the relative permittivity (relative dielectric
constant) of PMMA and c-PMMA gate dielectrics measured by impedance spectroscopy
while sweeping the ac frequency f_{ac} . The raw data and detailed extraction method are
provided in the Supporting Information.

Firstly, the relative permittivity of c-PMMA (3.9 at 10 kHz) is greater than PMMA (2.8),
which are close to the literature values 3.5 for c-PMMA³² and 2.5~2.9 for PMMA.³⁹ Based on
the Clausius-Mossotti equation⁴⁰ and effective medium theory,⁴¹ it was demonstrated that
the contribution of the free volume ($\epsilon_r \approx 1$) is strong and dominant in lowering the relative
permittivity of polymer dielectrics.⁴² Under this framework, the larger relative permittivity
of c-PMMA compared to PMMA is attributed to the significantly reduced free volume in
c-PMMA due to cross-linking. Together with the decreased thickness by one-fifth, the larger
relative permittivity of c-PMMA helps reducing the operating voltage.

In the meantime, noting that the dipolar polarization of the polar groups of the repeat-
ing units in the polymer composite is dominant in electronic applications ($f_{ac} < \text{GHz}$), it
can be inferred that the effect of the $\text{SiO}_{1.5}$ polar groups of polysilsesquioxane on relative
permittivity of c-PMMA is hardly discernible. This is because the molar and mass ratios of
the COOC polar pendant groups of PMMA chains are greater than these groups ($\text{SiO}_{1.5}$) as
3.4:1 and 3.9:1.

Secondly, similar dependence of relative permittivity on the ac frequency is observed
for both PMMA and c-PMMA gate dielectrics. At higher ac frequency, the direction of
the external electric field changes before the complete alignment of polar groups (for $f_{ac} <$

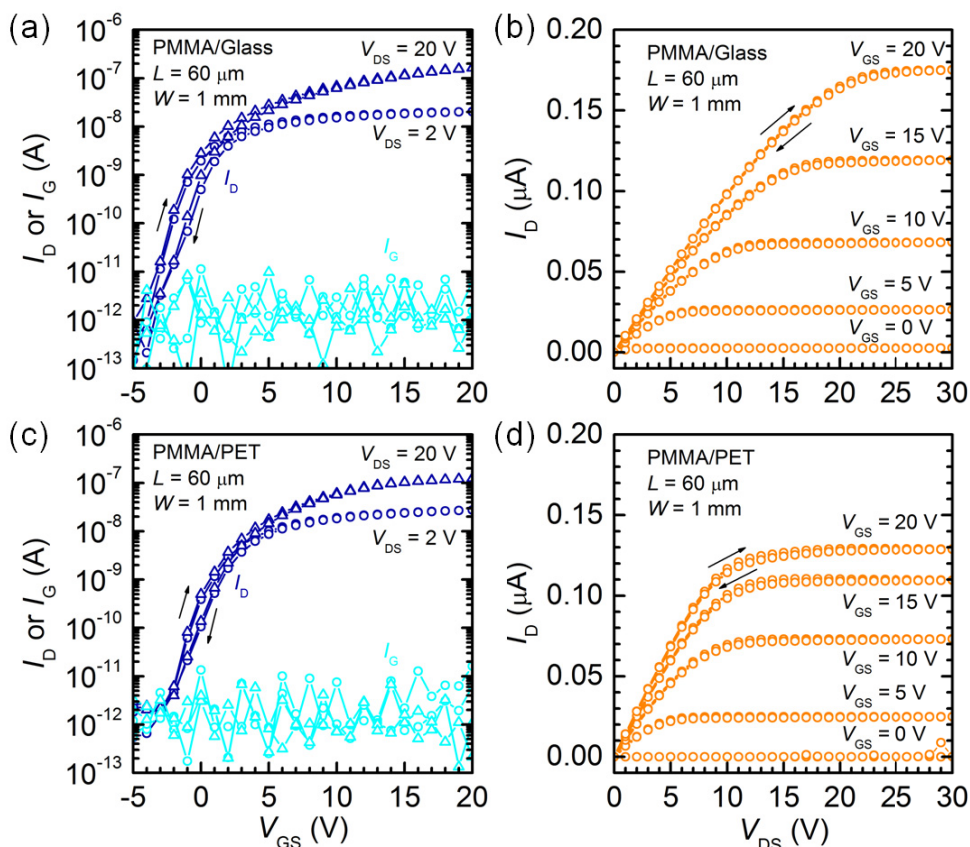


Figure 3: Linear and saturation regime transfer and output characteristics of *n*-type OFETs with PMMA fabricated on glass substrates (a) and (b) and on poly(ethylene terephthalate) (PET) substrates (c) and (d).

GHz) so that relative permittivity becomes smaller (i.e. less polarizable). In PMMA, the COOC polar pendant groups were reported to be responsible for the frequency dependence of relative permittivity.⁴³ A similar dependence of c-PMMA could be explained by (i) the minor contribution of the SiO_{1.5} polar groups present in smaller molar and mass ratios to COOC polar pendant groups of PMMA chains in the c-PMMA composite and (ii) the difficult rearrangement of SiO_{1.5} polar groups that are fixed in bridged polysilsesquioxane network.

3.2 *n*-Type OFETs with PMMA gate dielectric

Figure 3 shows the transfer and output characteristics of *n*-type OFETs with PMMA gate dielectric on glass (upper panels) and PET substrates (lower panels), where the data for

channel length $L = 60 \mu\text{m}$ are representatively shown.

In general, the materials (especially, the PMMA gate dielectric and n -type semiconductor), fabrication process and device structure are compatible with a flexible PET substrate. For n -type OFETs with PMMA on both substrates, the on-off drain current ratio ($I_{\text{on}}/I_{\text{off}}$) is large in the order of 10^5 with low gate leakage current $I_{\text{GS}} = 10^{-12}$ A. In spite of good transfer characteristics, however, a high operating voltage (~ 20 V) is needed.

On the other hand, focusing on the use of PMMA gate dielectric, it would be worth to mention a moderate lower back sweep current (BSC) hysteresis observed in n -type OFETs with PMMA on both substrates. The lower BSC hysteresis is very often attributed to charge carrier trapping close to the channel.⁴⁴ Thus, this gives evidence to the non-negligible amount of trap states for electrons in the organic semiconductor layer near gate dielectric rather than the trap sites in the gate dielectric layer (Recall the small RMS value of PMMA gate dielectric layer from Figure 2c).

Considering that the lower BSC is observed in OFETs with PMMA on both substrates (Figure 3) and that it is not observed in OFETs with c-PMMA gate on both substrates (Figure 4), it can be inferred that the density of trap states in the organic semiconductor layer close to the channel is more strongly related with the choice of gate dielectric rather than the choice of substrate. This indicates that the surface property of TIPS-TPDO-tetraCN is different on each gate dielectric (See Figures 5e-f for the comparison of TIPS-TPDO-tetraCN film morphology on different gate dielectric layers).

3.3 n -Type OFETs with c-PMMA gate dielectric

Figure 4 shows the transfer and output characteristics of n -type OFETs with c-PMMA gate dielectric on glass (upper panels) and PET substrates (lower panels), where the data for channel length $L = 60 \mu\text{m}$ are representatively shown.

A high on-off drain current ratio ($I_{\text{on}}/I_{\text{off}}$) in the order of 10^5 and low gate leakage current no greater than $I_{\text{GS}} = 10^{-10}$ A are maintained in n -type OFETs with c-PMMA gate

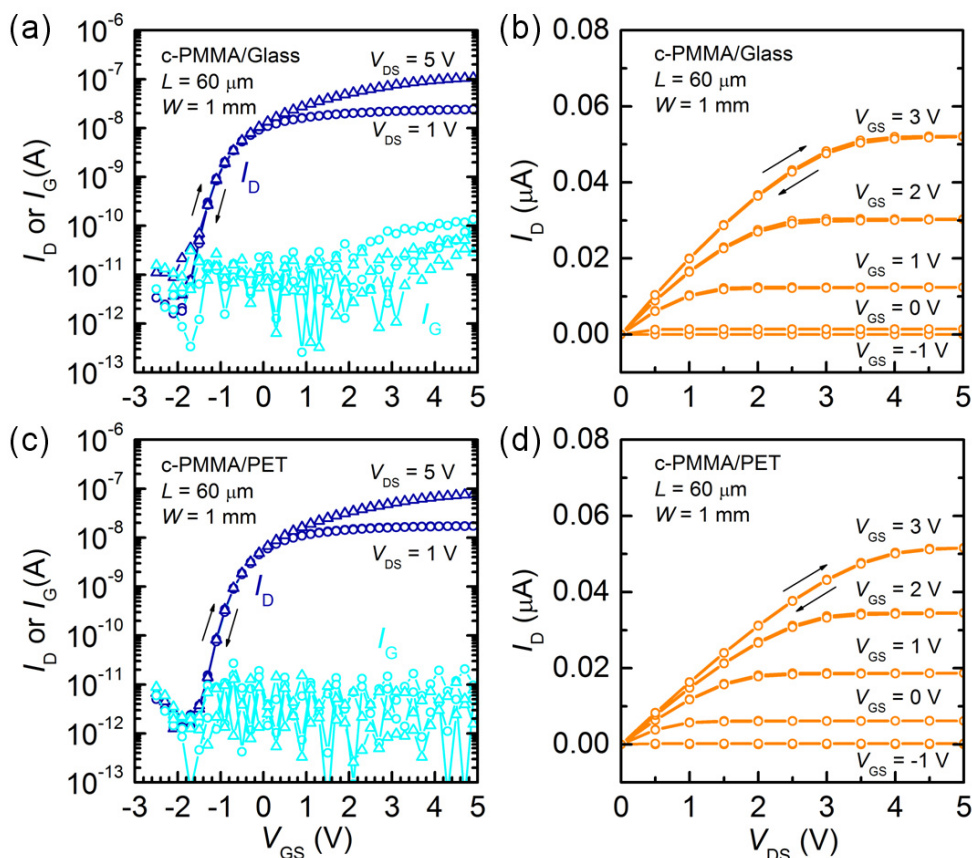


Figure 4: Linear and saturation regime transfer and output characteristics of *n*-type OFETs with c-PMMA fabricated on glass substrates (a) and (b) and on poly(ethylene terephthalate) (PET) substrates (c) and (d).

dielectric. Moreover, operating voltage is lowered down to few volts (~ 3 V, lower than one-fifth of 20 V) with a possibility for further improvements at the expense of the gate leakage current. This is due to higher relative permittivity and smaller thickness in the c-PMMA gate dielectric compared to PMMA gate dielectric.

Remarkably, in contrast to the *n*-type OFETs with PMMA gate dielectric, no hysteresis is observed on both substrates. This demonstrates a better semiconductor surface property on the c-PMMA gate dielectric than PMMA gate dielectric. This is co-evidenced by the larger electron mobility μ of *n*-type OFETs with c-PMMA gate dielectric (Figure 5). A more detailed comparison is made in the following sub-section.

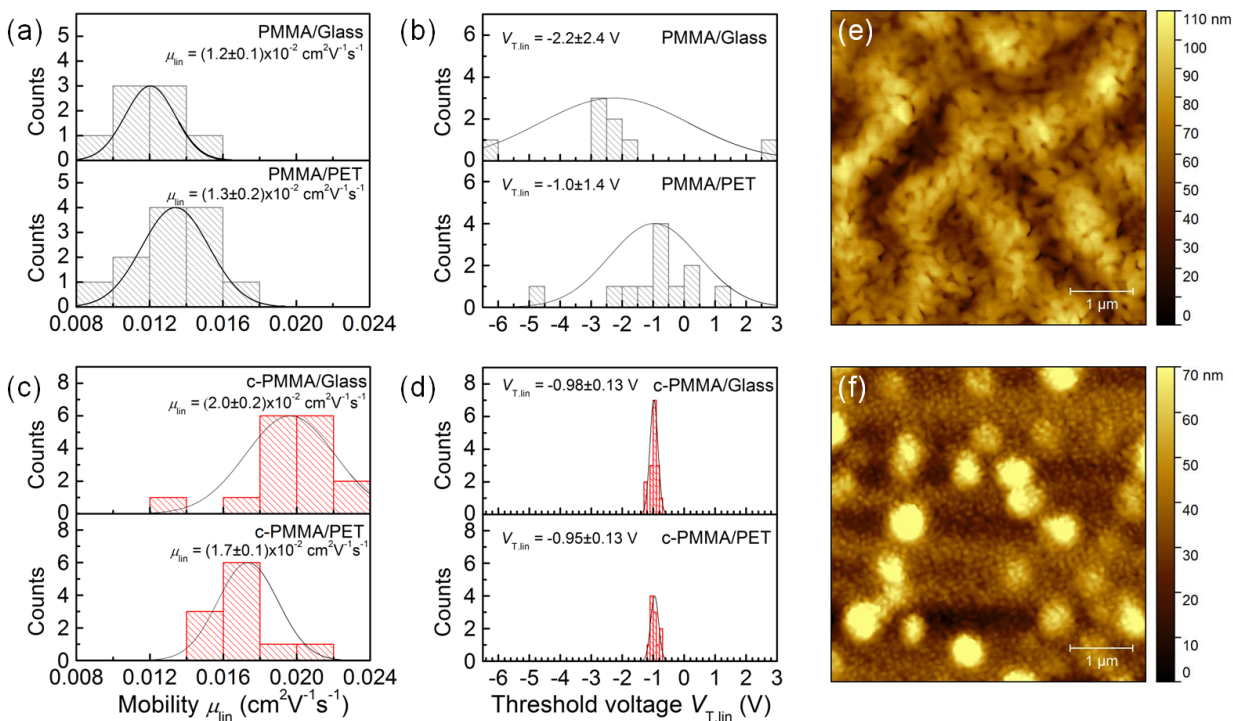


Figure 5: Histogram plots for linear regime field-effect mobility μ_{lin} and threshold voltage $V_{\text{T,lin}}$ of *n*-type OFETs: (a) and (b) with PMMA and (c) and (d) with c-PMMA (For each panel, glass and PET substrates are compared.) with tapping mode AFM images of TIPS-TPDO-tetraCN layer on (e) PMMA and (f) c-PMMA gate dielectric layer.

3.4 Device statistics

Figures 5a-d summarize two primary transistor parameters, electron mobility and threshold voltage extracted from linear regime transfer characteristics of TIPS-TPDO-tetraCN-based OFETs with the PMMA (upper panels) or c-PMMA (lower panels) gate dielectrics on the glass or PET substrates (divided into sub-panels). Each sub-panel contains data from OFETs on the same substrate. In total, there are 20 transistors on a substrate. The detailed extraction method can be found in the Supporting Information.

In terms of linear regime electron mobility μ_{lin} , the average values are larger in TIPS-TPDO-tetraCN-based OFETs with c-PMMA gate dielectrics $\mu_{\text{lin}} = (1.8 \pm 0.2) \times 10^{-2} \text{ cm}^2 \text{V}^{-1} \text{s}^{-1}$ compared to those with PMMA gate dielectric $\mu_{\text{lin}} = (1.2 \pm 0.2) \times 10^{-2} \text{ cm}^2 \text{V}^{-1} \text{s}^{-1}$. As briefly mentioned in Sec. 3.3, this indicates a better thin-film characteristics of organic semiconductor layer on c-PMMA gate dielectric. As shown in Figures 5e-f, both TIPS-TPDO-tetraCN

1
2
3
4
5
6
7
8
9
10
11
12
13
14
15
16
17
18
19
20
21
22
23
24
25
26
27
28
29
30
31
32
33
34
35
36
37
38
39
40
41
42
43
44
45
46
47
48
49
50
51
52
53
54
55
56
57
58
59
60

films on PMMA and c-PMMA exhibit small and uniform polycrystalline grains rather than pyramidal or dendritic grains. On PMMA, the film has grains in oval-shape with a long-axis length around 400 nm. On c-PMMA, the long-axis length is around 100 nm. In this island-mode growth,⁴⁵ a film with smaller grain size could have better inter-connected domains, which reduces inter-domain voids. Thus, the smaller grain size of TIPS-TPDO-tetraCN film on c-PMMA can explain its superior electron transporting behavior. On the other hand, standard deviation is comparable in both type of devices, which originates from the thermal evaporation process of organic semiconductor compatible to large area application.

For a rigorous analysis of linear regime threshold voltage $V_{T,lin}$, the effect of drain source voltage V_{DS} must be excluded by subtracting $V_{DS}/2$ from the threshold voltage extracted by linear-extrapolation method $V_{T,lin}^{eff}$ based on the following equation: $V_{T,lin}^{eff} = V_{T,lin} + V_{DS}/2$.⁴⁶ This becomes more important (i) for low-voltage OFETs, where drain source voltage V_{DS} is not negligibly smaller than gate source voltage V_{GS} and (ii) when comparing the linear regime threshold voltages of two OFETs applied with different V_{DS} .

While the average values is slightly larger in *n*-type OFETs with the PMMA gate dielectric compared to those with c-PMMA gate dielectric $V_{T,lin} = -1.6 \pm 2.0$ and -1.0 ± 0.13 V, the standard deviation of $V_{T,lin}$ is significantly reduced upon using c-PMMA gate dielectric approximately from 100% to 10% to the respective average values of $V_{T,lin}$. This highlights again a feasibility of the c-PMMA gate dielectric for large area applications. A higher yield of *n*-type OFETs with c-PMMA gate dielectric is also related to the homogeneity of the gate dielectric as previously mentioned in the literature.³²

3.5 Bending and air stability test

In order to assess the applicability of the TIPS-TPDO-tetraCN-based *n*-type OFETs on c-PMMA/PET for flexible electronics, the device stability was tested upon concave down bending with various radii from $r = \infty$ (after detach), 7 and 5 mm. The statistical analysis was conducted for four transistors on the same gate line. The transfer characteristics in linear

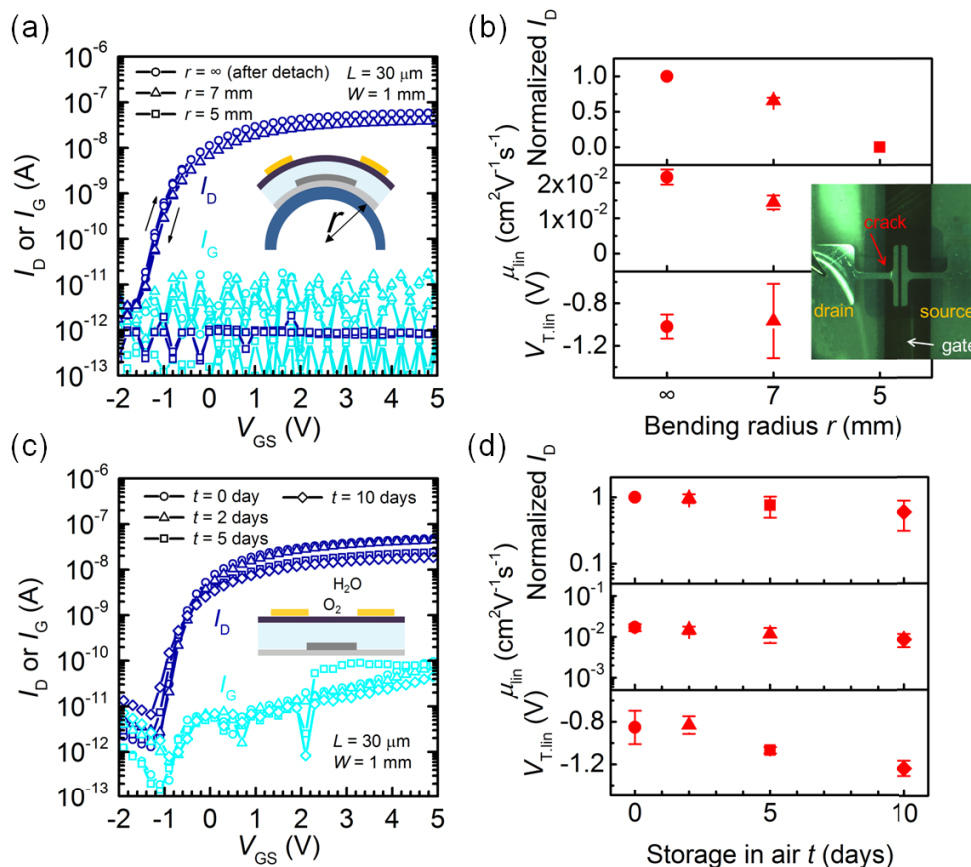


Figure 6: (a) Linear regime transfer characteristics of an OFET after detach, bending radius $r = 7$ and 5 mm. ($V_{DS} = 1$ V) (b) The changes in the normalized drain current I_D at $V_{GS} = 5$ V, linear mobility μ_{lin} and threshold voltage $V_{T,lin}$ upon bending (inset: top view optical image of an OFET bent at $r = 5$ mm showing a crack at the source metal contact). (c) Linear regime transfer characteristics of an OFET after storage in air and (d) consequent changes in device characteristics.

regime $V_{DS} = 1$ V were measured for all four transistors at certain bending radius before further bending. Figure 6a shows a representative transfer characteristic. As bending radius decreases, the device operates down to $r = 7$ mm with moderate degradation of transfer characteristics. From $r = 5$ mm, the transfer characteristics is not observed while the gate current remains unchanged, i.e. lower than 10^{-11} A.

Before device breakdown, upon bending at $r \leq 7$ mm, the average value of the normalized drain current read at $V_{GS} = 5$ V decreased 35% from 1 to 0.65 compared to $r = \infty$. Similarly, the average value of the linear regime mobility μ_{lin} decreased 37% from 2.2×10^{-2} to $1.4 \times$

1
2
3
4
5
6
7
8
9
10
11
12
13
14
15
16
17
18
19
20
21
22
23
24
25
26
27
28
29
30
31
32
33
34
35
36
37
38
39
40
41
42
43
44
45
46
47
48
49
50
51
52
53
54
55
56
57
58
59
60

$10^{-2} \text{ cm}^2\text{V}^{-1}\text{s}^{-1}$. For the linear regime threshold voltage $V_{T,\text{lin}}$, the standard deviation increased from 0.11 to 0.35 V although the average value was not changed. The degradation of mobility upon tensile strain similar to this study was reported in pentacene-based OFETs with polymer gate dielectrics, which was elucidated by less easier charge carrier hopping due to increased inter-molecular spacing.^{47,48} In addition, a concomitant morphological change at grain boundaries could be another possible origin.

The optical image (Figure 6b inset) of the device bent by $r = 5 \text{ mm}$ explains the device breakdown mechanism. A crack (red arrow) is observed at the neck of the drain contact. This is the origin of nearly constant drain current at 10^{-12} A which is the low limit of the current meter, while gate leakage current is still measurable around 10^{-11} A . This behavior is observed for all four transistors where the statistics is shown in Figure 6b.

A rough comparison (detailed in the Supporting Information) of the bending stability is possible between TIPS-TPDO-tetraCN-based *n*-type OFETs with c-PMMA gate dielectric on a PET ($175 \mu\text{m}$) substrate and pentacene-based *p*-type OFETs with a SAM/ AlO_x hybrid gate dielectric on a polyimide ($75 \mu\text{m}$) substrate (reported in the Supporting Information of a reference⁴⁹). For the pentacene-based OFET, the drain current decreases by 35% at $r = 2.2 \text{ mm}$ (corresponds to the strain $S = 1.71\%$) in pentacene layer. On the other hand, for the TIPS-TPDO-tetraCN-based OFET, the same degradation occurs at $r = 7 \text{ mm}$ ($S = 1.25\%$). Comparing the strain for a certain drain current degradation, it can be inferred that two devices have a comparable bending stability.

Finally, the air stability was tested from eight transistors. The device characteristics are maintained in air as shown in Figure 6c-d. The initial average values of linear mobility and threshold voltage in air are similar to those in nitrogen atmosphere: $\mu_{\text{lin}} = 1.7 \times 10^{-2} \text{ cm}^2\text{V}^{-1}\text{s}^{-1}$ and $V_{T,\text{lin}} = -0.85 \text{ V}$. After 10 days of storage in air, mobility remained high at $0.9 \times 10^{-2} \text{ cm}^2\text{V}^{-1}\text{s}^{-1}$ whereas threshold voltage showed a negative shift less than 0.4 V, which is strikingly stable for an evaporated thin-film.⁵⁰

4 Conclusion

We have demonstrated *n*-type OFETs based on a newly synthesized organic semiconductor (TIPS-TPDO-tetraCN) and a thin cross-linked polymer gate dielectric (*c*-PMMA). This approach enables linear regime electron mobility $(1.8\pm 0.2)\times 10^{-2} \text{ cm}^2\text{V}^{-1}\text{s}^{-1}$ and low operating voltage below 3V, while maintaining low gate leakage current no larger than 10^{-10} A . In addition, the linear regime threshold voltage $V_{T,\text{lin}} = -1.0\pm 0.13 \text{ V}$ has remarkably small spatial standard deviation. The device structure and fabrication process are compatible with a flexible PET substrate. In particular, efficient electron injection is possible from Au contact electrodes used commonly for hole injection in *p*-type semiconductor (pentacene). In addition, no hysteresis effect is observed in both transfer and output characteristics. All of aforementioned characteristics make the *n*-type OFET with TIPS-TPDO-tetraCN and *c*-PMMA a promising element for high-performance low-voltage organic complementary circuits.

Acknowledgement

This work has been funded by Horizon 2020 Marie Skłodowska-Curie Research and Innovation Staff Exchange (RISE) Programme (2015-2019) entitled DOMINO 645760. SJ acknowledges financial supports by the Vice Presidency for External Relations (DRI) of the École polytechnique (EP) through a Ph.D. fellowship. MA and TA thank Royal Saudi Naval Forces for financial supports for their studies in EP. GG acknowledges the Ph.D. fellowship from Université de Bordeaux. The Centre National de la Recherche Scientifique (CNRS), Agence Nationale de la Recherche (ANR) (FMOCSOLE ANR-BLAN-2010-93801), and the Institut Polytechnique de Bordeaux are acknowledged for financial support on the material development. Dr. Yassar, Abderrahim and Dr. Zucchi, Gaël are acknowledged for a fruitful discussion on *c*-PMMA.

Supporting Information Available

For further information on the impedance spectroscopy, FTIR spectroscopic Mueller ellipsometry and parameter extraction method and bending test for OFETs, please refer to the Supporting Information. This material is available free of charge via the Internet at <http://pubs.acs.org/>.

References

- (1) Tsumura, A.; Koezuka, H.; Ando, T. Macromolecular Electronic Device: Field-Effect Transistor With a Polythiophene Thin Film. *Appl. Phys. Lett.* **1986**, *49*, 1210–1212.
- (2) Guillaud, G.; Al Sadoun, M.; Maitrot, M.; Simon, J. Field-Effect Transistors Based on Intrinsic Molecular Semiconductors. *Chem. Phys. Lett.* **1990**, *167*, 503–506.
- (3) Tang, C. W. Two-layer Organic Photovoltaic Cell. *Appl. Phys. Lett.* **1986**, *48*, 183–185.
- (4) Tang, C. W.; VanSlyke, S. A. Organic Electroluminescent Diodes. *Appl. Phys. Lett.* **1987**, *51*, 913–915.
- (5) Greenham, N. C.; Moratti, S. C.; Bradley, D.; Friend, R. H. Efficient Light-Emitting Diodes Based on Polymers with High Electron Affinities. *Nature* **1993**, *365*, 628–630.
- (6) Hiramoto, M.; Fujiwara, H.; Yokoyama, M. p-i-n Like Behavior in Three-Layered Organic Solar Cells Having a Co-Deposited Interlayer of Pigments. *J. Appl. Phys.* **1992**, *72*, 3781–3787.
- (7) Strukelj, M.; Papadimitrakopoulos, F.; Miller, T. M.; Rothberg, L. J. Design and Application of Electron-Transporting Organic Materials. *Science* **1995**, *267*, 1969–1972.
- (8) Paloheimo, J.; Isotalo, H.; Kastner, J.; Kuzmany, H. Conduction Mechanisms in Undoped Thin Films of C60 and C60/70. *Synth. Met.* **1993**, *56*, 3185–3190.

- 1
2
3
4 (9) Hoshimono, K.; Fujimori, S.; Fujita, S.; Fujita, S. Semiconductor-Like Carrier Conduc-
5 tion and Its Field-Effect Mobility in Metal-Doped C60 Thin Films. *Jpn. J. Appl. Phys.*
6 **1993**, *32*, L1070–L1073.
7
8
9
10 (10) Haddon, R. C.; Perel, A. S.; Morris, R. C.; Palstra, T. T. M.; Hebard, A. F.; Flem-
11 ing, R. M. C60 Thin Film Transistors. *Appl. Phys. Lett.* **1995**, *67*, 121–123.
12
13
14 (11) Horowitz, G.; Kouki, F.; Spearman, P.; Fichou, D. Evidence for n-Type Conduction in
15 a Perylene Tetracarboxylic Diimide Derivative. *Adv. Mater.* **1996**, *8*, 242–245.
16
17
18 (12) Bode, D.; Rolin, C.; Schols, S.; Debucquoy, M.; Steudel, S.; Gelinck, G. H.; Genoe, J.;
19 Heremans, P. Noise-Margin Analysis for Organic Thin-Film Complementary Technol-
20 ogy. *IEEE Trans. Electron Devices* **2009**, *57*, 201–208.
21
22
23 (13) Ng, T. N.; Schwartz, D. E.; Lavery, L. L.; Whiting, G. L.; Russo, B.; Krusor, B.;
24 Veres, J.; Bröms, P.; Herlogsson, L.; Alam, N.; Hagel, O.; Nilsson, J.; Karlsson, C.
25 Scalable Printed Electronics: an Organic Decoder Addressing Ferroelectric Non-Volatile
26 memory. *Sci. Rep.* **2012**, *2*, 1–7.
27
28
29 (14) Klauk, H. Organic Thin-Film Transistors. *Chem. Soc. Rev.* **2010**, *39*, 2643–2666.
30
31
32 (15) Zhao, Y.; Guo, Y.; Liu, Y. 25th Anniversary Article: Recent Advances in n-Type and
33 Ambipolar Organic Field-Effect Transistors. *Adv. Mater.* **2013**, *25*, 5372–5391.
34
35
36 (16) Klauk, H.; Halik, M.; Zschieschang, U.; Eder, F.; Rohde, D.; Schmid, G.; Dehm, C.
37 Flexible Organic Complementary Circuits. *IEEE Trans. Electron Devices* **2005**, *52*,
38 618–622.
39
40
41 (17) Jones, B. A.; Facchetti, A.; Wasielewski, M. R.; Marks, T. J. Tuning Orbital Energetics
42 in Arylene Diimide Semiconductors. Materials Design for Ambient Stability of n-Type
43 Charge Transport. *J. Am. Chem. Soc.* **2007**, *129*, 15259–15278.
44
45
46
47
48
49
50
51
52
53
54
55
56
57
58
59
60

- 1
2
3
4
5
6
7
8
9
10
11
12
13
14
15
16
17
18
19
20
21
22
23
24
25
26
27
28
29
30
31
32
33
34
35
36
37
38
39
40
41
42
43
44
45
46
47
48
49
50
51
52
53
54
55
56
57
58
59
60
- (18) Oh, J. H.; Suraru, S.-L.; Lee, W.-Y.; Könemann, M.; Höffken, H. W.; Röger, C.; Schmidt, R.; Chung, Y.; Chen, W.-C.; Würthner, F.; Bao, Z. High-Performance Air-Stable n-Type Organic Transistors Based on Core-Chlorinated Naphthalene Tetracarboxylic Diimides. *Adv. Funct. Mater.* **2010**, *20*, 2148–2156.
- (19) Soeda, J.; Uemura, T.; Mizuno, Y.; Nakao, A.; Nakazawa, Y.; Facchetti, A.; Takeya, J. High Electron Mobility in Air for N,N-1H,1H-Perfluorobutyldicyanoperylene Carboxydi-imide Solution-Crystallized Thin-Film Transistors on Hydrophobic Surfaces. *Adv. Mater.* **2011**, *23*, 3681–3685.
- (20) Chung, Y.; Verploegen, E.; Vailionis, A.; Sun, Y.; Nishi, Y.; Murmann, B.; Bao, Z. Controlling Electric Dipoles in Nanodielectrics and Its Applications for Enabling Air-Stable n-Channel Organic Transistors. *Nano Lett.* **2011**, *11*, 1161–1165.
- (21) Senanayak, S. P.; Sangwan, V. K.; McMorro, J. J.; Everaerts, K.; Chen, Z.; Facchetti, A.; Hersam, M. C.; Marks, T. J.; Narayan, K. S. Self-Assembled Nanodielectrics for High-Speed, Low-Voltage Solution-Processed Polymer Logic Circuits. *Adv. Electron. Mater.* **2015**, *1*, 1500226.
- (22) Di, C.-a.; Li, J.; Yu, G.; Xiao, Y.; Guo, Y.; Liu, Y.; Qian, X.; Zhu, D. Trifluoromethyl-triphenodioxazine: Air-Stable and High-Performance n-Type Semiconductor. *Organic Letters* **2008**, *10*, 3025–3028.
- (23) Nicolas, Y.; Castet, F.; Devynck, M.; Tardy, P.; Hirsch, L.; Labrugère, C.; Allouchi, H.; Toupance, T. TIPS-triphenodioxazine versus TIPS-pentacene: Enhanced Electron Mobility for n-Type Organic Field-Effect Transistors. *Org. Electron.* **2012**, *13*, 1392–1400.
- (24) Gruntz, G.; Lee, H.; Hirsch, L.; Castet, F.; Toupance, T.; Briseno, A. L.; Nicolas, Y. Nitrile Substitution Effect on Triphenodioxazine-Based Materials for Liquid-Processed Air-Stable n-Type Organic Field Effect Transistors. *Adv. Electron. Mater.* **2015**, 1500072.

- 1
2
3
4 (25) Horowitz, G.; Delannoy, P. An Analytical Model for Organic-Based Thin-Film Tran-
5 sistors. *J. Appl. Phys.* **1991**, *70*, 469–475.
6
7
8
9 (26) Lin, W.-Y.; Müller, R.; Myny, K.; Steudel, S.; Genoe, J.; Heremans, P. Room-
10 Temperature Solution-Processed High-k Gate Dielectrics for Large Area Electronics
11 Applications. *Org. Electron.* **2011**, *12*, 955–960.
12
13
14
15 (27) Vuillaume, D.; Boulas, C.; Collet, J.; Davidovits, J. V.; Rondelez, F. Organic Insulating
16 Films of Nanometer Thicknesses. *Appl. Phys. Lett.* **1996**, *69*, 1646–1648.
17
18
19
20 (28) Klauk, H.; Zschieschang, U.; Pflaum, J.; Halik, M. Ultralow-Power Organic Comple-
21 mentary Circuits. *Nature* **2007**, *445*, 745–748.
22
23
24
25 (29) Ha, Y.-G.; Emery, J. D.; Bedzyk, M. J.; Usta, H.; Facchetti, A.; Marks, T. J. Solution-
26 Deposited Organic–Inorganic Hybrid Multilayer Gate Dielectrics. Design, Synthesis,
27 Microstructures, and Electrical Properties with Thin-Film Transistors. *J. Am. Chem.*
28 *Soc.* **2011**, *133*, 10239–10250.
29
30
31
32
33
34 (30) Yoon, M.-H.; Yan, H.; Facchetti, A.; Marks, T. J. Low-Voltage Organic Field-Effect
35 Transistors and Inverters Enabled by Ultrathin Cross-Linked Polymers as Gate Di-
36 electrics. *J. Am. Chem. Soc.* **2005**, *127*, 10388–10395.
37
38
39
40
41 (31) Kim, C.; Wang, Z.; Choi, H.-J.; Ha, Y.-G.; Facchetti, A.; Marks, T. J. Printable Cross-
42 Linked Polymer Blend Dielectrics. Design Strategies, Synthesis, Microstructures, and
43 Electrical Properties, with Organic Field-Effect Transistors as Testbeds. *J. Am. Chem.*
44 *Soc.* **2008**, *130*, 6867–6878.
45
46
47
48
49
50 (32) Noh, Y.-Y.; Sirringhaus, H. Ultra-Thin Polymer Gate Dielectrics for Top-Gate Polymer
51 Field-Effect Transistors. *Org. Electron.* **2009**, *10*, 174–180.
52
53
54
55 (33) Loffredo, F.; Grimaldi, I. A.; Miscioscia, R.; Nenna, G.; Villani, F.; Minarini, C.;
56 Petrosino, M.; Rubino, A.; Usta, H.; Facchetti, A. Photosensing Properties of Pentacene
57
58
59
60

- 1
2
3 OFETs Based on a Novel PMMA Copolymer Gate Dielectric. *J. Disp. Technol.* **2015**,
4 *11*, 533–540.
5
6
7
8
9 (34) Kraft, U.; Sejfić, M.; Kang, M. J.; Takimiya, K.; Zaki, T.; Letzkus, F.; Burghartz, J. N.;
10 Weber, E.; Klauk, H. Flexible Low-Voltage Organic Complementary Circuits: Finding
11 the Optimum Combination of Semiconductors and Monolayer Gate Dielectrics. *Adv.*
12 *Mater.* **2014**, *27*, 207–214.
13
14
15
16
17 (35) Yang, Y. S.; You, I. K.; Koo, J. B.; Lee, S. S.; Lim, S. C.; Kang, S. Y. Characteristics of
18 Via-Hole Interconnections Fabricated by Using an Inkjet Printing Method. *J. Korean*
19 *Phys. Soc.* **2010**, *57*, 1699–1701.
20
21
22
23
24 (36) Shea, K. J.; Moreau, J.; Loy, D. A.; Corriu, R. J. P.; Boury, B. In *Functional Hybrid*
25 *Materials*, 2nd ed.; Gómez-Romero, P., Sanchez, C., Eds.; Wiley-VCH Verlag GmbH
26 & Co. KGaA: Weinheim, FRG, 2005; pp 50–85.
27
28
29
30
31 (37) Launer, P. J. In *Silicone Compounds Register and Review*, 4th ed.; Arkles, B. C., Pe-
32 terson, W. R., Eds.; Petrarch Systems: Bristol, PA, 1987; pp 100–103.
33
34
35
36 (38) Smith, B. C. *Infrared Spectral Interpretation: A Systematic Approach*, 1st ed.; CRC
37 Press: Boca Raton, FL, 1998; pp 108–114.
38
39
40
41 (39) Park, J. H.; Hwang, D. K.; Lee, J.; Im, S.; Kim, E. Studies on Poly(methyl methacry-
42 late) Dielectric Layer for Field Effect Transistor: Influence of Polymer Tacticity. *Thin*
43 *Solid Films* **2007**, *515*, 4041–4044.
44
45
46
47
48 (40) Kittel, C. *Introduction to Solid State Physics*, 8th ed.; Wiley: New York, 2004.
49
50
51 (41) Choy, T. C. *Effective Medium Theory*, 1st ed.; Clarendon Press: Oxford, 1999.
52
53
54 (42) Hougham, G.; Tesoro, G.; Viehbeck, A. Influence of Free Volume Change on the Rela-
55 tive Permittivity and Refractive Index in Fluoropolyimides. *Macromolecules* **1996**, *29*,
56 3453–3456.
57
58
59
60

- 1
2
3
4 (43) Pillai, P.; Khurana, P.; Tripathi, A. Dielectric Studies of Poly(methyl methacry-
5 late)/Polystyrene Double Layer System. *J. Mater. Sci. Lett.* **1986**, *5*, 629–632.
6
7
8
9 (44) Egginger, M.; Bauer, S.; Schwödiauer, R.; Neugebauer, H.; Sariciftci, N. S. Current
10 Versus Gate Voltage Hysteresis in Organic Field Effect Transistors. *Monatsh. Chem.*
11 **2009**, *140*, 735–750.
12
13
14
15 (45) Yang, S. Y.; Shin, K.; Park, C. E. The Effect of Gate-Dielectric Surface Energy on
16 Pentacene Morphology and Organic Field-Effect Transistor Characteristics. *Adv. Funct.*
17 *Mater.* **2005**, *15*, 1806–1814.
18
19
20
21
22 (46) Jung, S.; Kim, C. H.; Bonnassieux, Y.; Horowitz, G. Fundamental Insights into the
23 Threshold Characteristics of Organic Field-Effect Transistors. *J. Phys. D: Appl. Phys.*
24 **2015**, *48*, 035106.
25
26
27
28
29 (47) Sekitani, T.; Iba, S.; Kato, Y.; Someya, T. Bending Effect of Organic Field-Effect
30 Transistors with Polyimide Gate Dielectric Layers. *Jpn. J. Appl. Phys.* **2005**, *44*, 2841–
31 2843.
32
33
34
35
36 (48) Sokolov, A. N.; Cao, Y.; Johnson, O. B.; Bao, Z. Mechanistic Considerations of Bending-
37 Strain Effects within Organic Semiconductors on Polymer Dielectrics. *Adv. Funct.*
38 *Mater.* **2012**, *22*, 175–113.
39
40
41
42
43 (49) Sekitani, T.; Zschieschang, U.; Klauk, H.; Someya, T. Flexible Organic Transistors and
44 Circuits with Extreme Bending Stability. *Nat. Mater.* **2010**, *9*, 1–8.
45
46
47
48 (50) Weitz, R. T.; Amsharov, K.; Zschieschang, U.; Burghard, M.; Jansen, M.; Kelsch, M.;
49 Rhamati, B.; van Aken, P. A.; Kern, K.; Klauk, H. The Importance of Grain Boundaries
50 for the Time-Dependent Mobility Degradation in Organic Thin-Film Transistors. *Chem.*
51 *Mater.* **2009**, *21*, 4949–4954.
52
53
54
55
56
57
58
59
60

Graphical TOC Entry

